Equilibrium Orientation of Nonspherical Janus Particles at Fluid–Fluid Interfaces

Bum Jun Park and Daeyeon Lee*

Department of Chemical and Biomolecular Engineering, University of Pennsylvania, Philadelphia, Pennsylvania 19104, United States

ABSTRACT We study the equilibrium orientation of nonspherical Janus particles at an oil–water interface. Two types of nonspherical Janus particles are considered: Janus ellipsoids and Janus dumbbells. To find their equilibrium orientation, we calculate and minimize the attachment energy of each Janus particle as a function of its orientation angle with respect to the oil–water interface. We find that the equilibrium orientation of the interface trapped Janus particles strongly depends on the particle characteristics, such as their size, aspect ratio, and surface properties. In general, nonspherical Janus particles adopt the upright orientation (*i.e.*, the long axis of ellipsoids or dumbbells is perpendicular to the interface) if the difference in the wettability of the two sides is large or if the particle aspect ratio is close to 1. In contrast, Janus particles with a large aspect ratio or a small difference in the wettability of the two regions tend to have a tilted orientation at equilibrium. Moreover, we find that Janus ellipsoids, under appropriate conditions, can be kinetically trapped in a metastable state due to the presence of a secondary energy minimum. In contrast, Janus dumbbells possess only a primary energy minimum, indicating that these particles prefer to be in a single orientation. The absence of a secondary minimum is potentially advantageous for obtaining particle layers at fluid–fluid interfaces with uniform orientation. Our calculation provides a detailed guidance for synthesizing nonspherical Janus particles that can be used as effective solid surfactants for the stabilization of multiphasic fluid mixtures and the modification of the rheological properties of fluid interfaces.

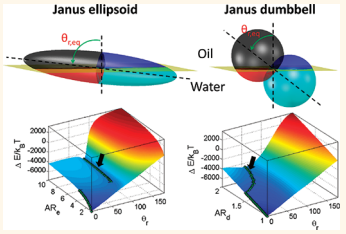

KEYWORDS: colloid · interface · attachment energy · Janus particle · equilibrium orientation

Janus particles have two sides that have different, often opposite, surface properties.[1–4] Each side of the Janus particles can be modified independently to tailor their assembly behaviors in a fluid.[5–14] Janus particles also have been studied as autonomous motors that can propel themselves through fluids under the influence of an external field or a catalytic reaction.[15–17] Moreover, amphiphilic Janus spheres have been shown to adsorb strongly to fluid–fluid interfaces, making them effective emulsion stabilizers.[11,18–20]

Recent progress has enabled the synthesis of nonspherical Janus particles, which possess an additional degree of freedom in tuning the particle characteristics.[17,21–32] For example, Janus paramagnetic ellipsoids have been shown to exhibit unique responses to a rotating magnetic field.[22] The aspect ratio of these ellipsoidal particles can be readily tuned using a mechanical stretching method.[33–36] A study has also shown that Janus magnetic nanorods spontaneously assemble at the interface of water-in-oil emulsions to form magnetic field-responsive colloidosomes. The stability of these colloidosomes were shown to depend on the aspect ratio of the nanorods.[27] Another type of nonspherical Janus particles that have garnered much interest recently is Janus dumbbells, which comprise two partially fused spheres.[23–25,37] By independently controlling the size ratio of the two spheres and the wettability of each sphere, their assembly behavior in a fluid can be controlled. A recent study has suggested the use of the "packing parameter" concept to describe their assembly behavior, analogous to the packing parameter argument that has successfully described the assembly of amphiphilic molecules.[24,38]

One of the most intriguing applications of Janus particles is the stabilization of multiphasic fluid mixtures such as emulsions and bubbles because these particles attach to the interfaces more efficiently than their homogeneous counterparts.[2,3,18,19,27,31,39–41] Recent studies strongly suggest that the geometry as well as the surface properties of nonspherical Janus particles have a significant influence on their surface activity.[27,31,42] Understanding the effect of geometry and surface properties will be critical in effectively utilizing these particles as solid surfactants in the stabilization of multiphasic systems.[24] Despite the importance of geometry and surface wettability, few design criteria currently exist that can aid the synthesis of nonspherical Janus particles that can function as effective solid surfactants. For example, the importance of controlling the particle size is not well understood. It is not clearly

* Address correspondence to daeyeon@seas.upenn.edu.

Received for review November 3, 2011 and accepted December 20, 2011.

Published online December 20, 2011
10.1021/nn204261w

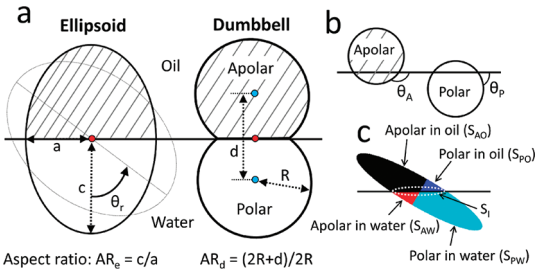

Figure 1. (a) Geometry of nonspherical Janus particles at a planar oil–water interface. The apolar region of Janus particles is represented by the shaded region. The aspect ratio of a Janus ellipsoid is defined as $AR_e = c/a$, where c and a denote the radii of long- and short-axes (*e.g.*, $AR_e = 1$ is a sphere). Janus dumbbells consist of two partially fused spheres with a center-to-center (blue dots) separation of d between them. The aspect ratio of a Janus dumbbell is defined as $AR_d = (2R + d)/2R$, where R is the radius of the polar and apolar spheres (*e.g.*, $AR_d = 1$ and 2 correspond to a sphere and two contacting spheres, respectively). Each Janus particle rotates by θ_r around a rotational axis represented by the center of mass (red point) in each case. (b) θ_A and θ_P are the three-phase contact angles of apolar and polar spherical particles at the oil–water interface, respectively. (c) A Janus ellipsoid at the oil–water interface; different colors represent four different particle surface–fluid interfaces: (black) apolar surface in contact with oil (S_{AO}), (red) apolar surface in contact with water (S_{AW}), (blue) polar surface in contact with oil (S_{PO}), and (cyan) polar surface in contact with water (S_{PW}). The white dotted line indicates the cross-sectional area of the particle intersected by the oil–water interface (S_I).

known whether it is advantageous to synthesize and use nanometer-scale nonspherical Janus particles as opposed to micrometer-scale particles. Most theoretical work, to date, has focused on understanding the behavior of spherical Janus particles, such as their equilibrium orientation, at fluid–fluid interfaces.[1−4,18,19,40,41] We believe it is critical, at this stage, to provide a quantitative analysis of the equilibrium orientation of nonspherical Janus particles to enable effective utilization of this unique family of colloids.

In this paper, we determine the equilibrium orientation of Janus particles with chemical (*i.e.*, surface energy) and geometric (*i.e.*, ellipsoids and dumbbells) heterogeneity at an oil–water interface. We numerically calculate the surface area of the particle in each fluid phase and the area of the oil–water interface occupied by the particle. The calculated area and the surface energy of the two sides of Janus particles determine the attachment energy as a function of orientation angle with respect to the interface. We study the effect of the aspect ratio, surface wettability, and size of nonspherical Janus particles on their equilibrium orientation. The results presented in this study provide critical guidelines and insights into synthesizing nonspherical Janus particles for applications involving fluid–fluid interfaces.

RESULTS AND DISCUSSION

Geometry and Surface Properties of Nonspherical Janus Particles. We study the equilibrium orientation of Janus ellipsoids and dumbbells trapped at an oil–water interface. As described above, these Janus particles have been recently synthesized, and their behavior and properties have been shown to depend strongly on their geometry and wettability.[22−25,37] The geometries of Janus ellipsoids and dumbbells used in this study are shown in Figure 1a. Unless otherwise noted, the surface area of both the ellipsoids and the dumbbells is set to $S_0 = 4\pi(10\text{ nm})^2$, which corresponds to that of a sphere with the radius of 10 nm.

The Janus ellipsoids and dumbbells we study in this work have two regions of opposite surface wettability: apolar and polar (Figure 1a). The boundary between the two regions is called the Janus boundary.[43] The Janus boundary of Janus ellipsoids is located at the intersection of the surface of the ellipsoid and the plane that is perpendicular to ellipsoid's long axis and that contains the ellipsoid's center of mass.[43] The boundary between the two spheres comprising Janus dumbbells is the Janus boundary.[23,24] Each Janus particle rotates with respect to a pivot represented by a red dot in Figure 1a. The orientation angle (θ_r) is defined as the angle between the long-axis of a Janus particle in the upright orientation and that in a rotated orientation. For example, orientation angles of $\theta_r = 0°$ and 90° correspond to the Janus boundary being parallel (upright orientation) and perpendicular (horizontal orientation) to the oil–water interface, respectively.

The surface wettability of the apolar and polar regions of Janus particles is represented by the three-phase contact angles, θ_A and θ_P, respectively, as shown in Figure 1b. The calculations presented in this study are based on the two regions of opposite wettability (*i.e.*, apolar and polar), represented by $\theta_A = 90° + \beta$ and $\theta_P = 90° - \beta$. This indicates that the center of mass of these Janus particles, at equilibrium, will be located at the oil–water interface, regardless of the values of β and θ_r. Therefore, the vertical displacement of the Janus particles is negligible. For a given orientation of a Janus particle at the oil–water interface, the surface of a Janus particle is divided into four regions as shown in Figure 1c. The corresponding surface areas are numerically calculated as will be discussed in the Methods section.

In this study, we assume that the superphase is decane (oil) and the subphase is water. This decane–water interface system has been widely used for studying the behavior of particles at fluid–fluid interfaces.[43−47] The interfacial tension ($\gamma_{OW} = 50$ mN/m) between the two fluids has been measured by the pendant drop method.[45,47] Note that other fluid–fluid interfaces (*e.g.*, air–water interface) can be used in our calculations by using the appropriate values of interfacial tension (*e.g.*, $\gamma_{AW} = 72$ mM/m) and surface energy.

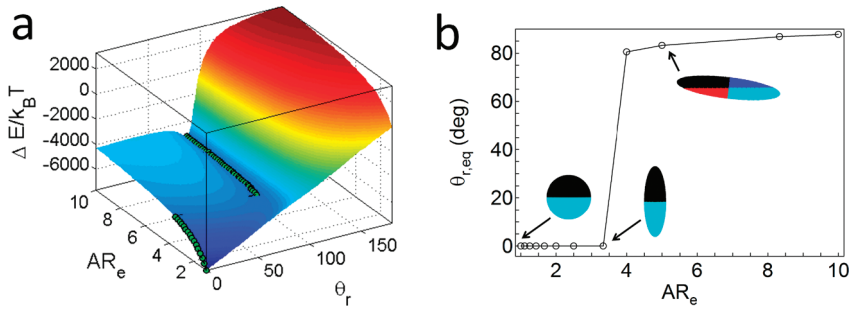

Figure 2. (a) Three-dimensional (3D) contour plot of attachment energy (ΔE) of Janus ellipsoids with $\beta = 30°$ as a function of aspect ratio (AR_e) and rotational angle (θ_r). Each green symbol on the contour surface represents the global energy minimum (ΔE_{eq}) for a given value of AR_e between 1 and 10. (b) Equilibrium orientations ($\theta_{r,eq}$) as a function of AR_e. The schematics of spheres and ellipsoids in Figure 2b show their equilibrium orientations at the oil−water interface.

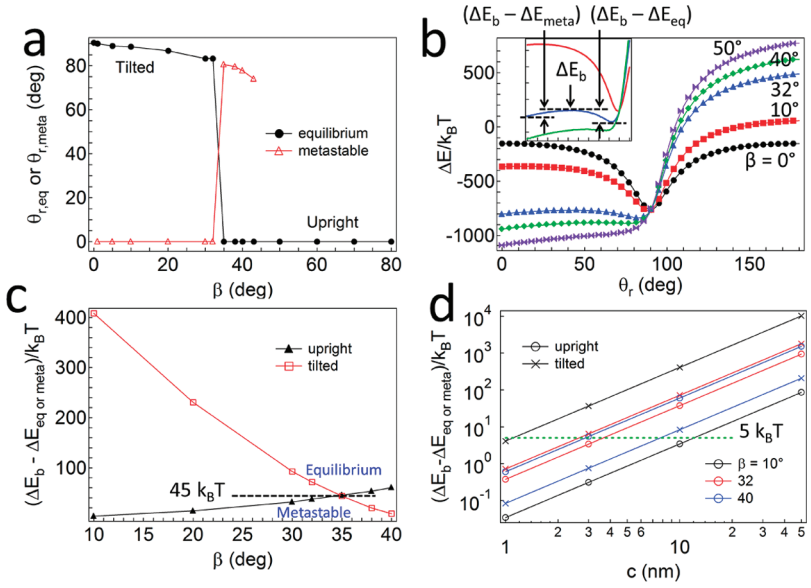

Figure 3. (a) Variation of the equilibrium ($\theta_{r,eq}$) and metastable orientations ($\theta_{r,meta}$) of Janus ellipsoids with $AR_e = 5$ and $c = 10$ nm as a function of β. (b) Attachment energy (ΔE) as a function of θ_r and β. The inset is a magnified plot to illustrate the magnitude of the energy barrier between equilibrium and metastable orientations. (c) Magnitude of the energy barriers from upright ($\theta_{r,eq} \approx 0°$) to tilted ($\theta_{r,eq} \neq 0°$) and from tilted to upright orientations as a function of β. (d) Effect of the size of Janus ellipsoids on $\Delta E_b - \Delta E_{eq}$ and $\Delta E_b - \Delta E_{meta}$. The green dotted line represents a guide line for 5 k_BT.

Janus Ellipsoids. The aspect ratio of Janus ellipsoids has a significant influence on their equilibrium orientation. We illustrate this observation using Janus ellipsoids with $\beta = 30°$.[48] The attachment energy of Janus ellipsoids as a function of orientation angle (θ_r) and aspect ratio (AR_e) is shown in Figure 2a.[49] The equilibrium energy minima (ΔE_{eq}) as a function of AR_e are represented by green symbols on the three-dimensional (3D) contour surface. The global energy minimum (ΔE_{eq}) for $AR_e = 1$ (*i.e.*, spherical Janus particle) occurs at $\theta_{r,eq} \approx 0°$; however, as AR_e is increased above 3.3, the equilibrium orientation ($\theta_{r,eq}$) becomes larger than 80°, which we discuss in detail below.

As shown in Figure 2b, for a spherical Janus particle ($AR_e = 1$, $\beta = 30°$), the equilibrium orientation, determined by locating the global energy minimum, corresponds to the case with the Janus boundary pinned at the oil−water interface, and the apolar and polar hemispheres exposed to the oil and water phases, respectively (*i.e.*, $\theta_{r,eq} \approx 0°$ in Figure 2b). This result is consistent with previous results based on experiments[43,50] and theoretical considerations.[3,18,19,39,40] If the spherical Janus particle is rotated out of its equilibrium position, which can be conveniently performed in a theoretical calculation, the magnitude of attachment energy linearly decreases (Figure 2a) as a function of rotation angle (θ_r).

The aspect ratio (AR_e) of Janus ellipsoids ($\beta = 30°$) has a significant impact on their equilibrium orientation ($\theta_{r,eq}$) as summarized in Figure 2b. For AR_e between 1 and 3.3, the oil−water interface is pinned at the Janus boundary. The Janus boundary abruptly rotates out of the oil−water interface plane (*i.e.*, tilted orientation) for higher values of AR_e (*i.e.*, $AR_e \geq 4$). In the case of a Janus ellipsoid with the aspect ratio of $AR_e = 5$, the Janus boundary of the particle at

equilibrium is no longer in the same plane as the oil–water interface (*i.e.*, $\theta_{r,eq} \approx 83°$) as seen in Figure 2b. This result suggests that as AR_e increases, the equilibrium orientation of Janus ellipsoids is dominated by the tendency to increase the cross-sectional area (S_I in Figure 1c) of the particle intersected by the oil–water interface and, in turn, the magnitude of the attachment energy (see eq 7).

The equilibrium orientation of a high aspect ratio Janus ellipsoid ($AR_e = 5$) depends strongly on the wettability of the two regions (*i.e.*, β). As shown in Figure 3a, if the difference in the wettability of the apolar and polar regions is large (*i.e.*, $\beta \geq 35°$), the ΔE_{eq} is observed at $\theta_{r,eq} = 0°$, which is the upright orientation. If the wettability difference is not very large (*i.e.*, $\beta < 35°$), such Janus ellipsoids prefer to be in a tilted orientation with its long-axis almost parallel to the oil–water interface (Figure 3a). This drastic change in the equilibrium orientation (*i.e.*, from the tilted orientation to the upright one) for the high values of β is due to the particle's tendency to maximize the magnitude of the attachment energy by increasing the interfacial area between each region of the particle and its preferred fluid phase (*i.e.*, apolar in oil, S_{AO}, and polar in water, S_{PW}, in Figure 1c (see also eq 7)).

Interestingly, for the high aspect ratio Janus ellipsoids with $AR_e = 5$ and $c = 10$ nm, two energy minima are found as a function of orientation angle (θ_r). This result indicates that these Janus ellipsoids can be kinetically trapped in a metastable orientation (*i.e.*, secondary minimum). Figure 3b shows the attachment energy profiles (ΔE) as a function of θ_r and β. The primary and secondary energy minima as well as the energy barrier (ΔE_b) between the equilibrium and metastable states appear when β is between 1° and 43° (Figure 3a,b). As shown in Figure 3a, for $35° \leq \beta \leq 43°$, the equilibrium orientation is observed at $\theta_{r,eq} \approx 0°$ at which the particle is stable in the upright orientation with the Janus boundary pinned at the oil–water interface; the corresponding attachment energy is ΔE_{eq} (Figure 3b). A metastable state is observed at $\theta_{r,meta} \approx 80°$, close to the horizontal orientation, where the attachment energy is ΔE_{meta} (Figure 3b). In contrast, for $1° \leq \beta \leq 32°$, the tilted and upright orientations correspond to the equilibrium and metastable energy states, respectively. For $\beta \geq 50°$, only primary energy minimum exists at the upright orientation; thus, these Janus ellipsoids do not have metastable orientations (Figure 3a).

The orientation of Janus ellipsoids is predicted to be significantly influenced by the magnitude of the energy barrier between the equilibrium and metastable states. For Janus ellipsoids with $\beta = 35°$ and $AR_e = 5$, the difference in the attachment energy between the equilibrium and metastable orientations is very small ($|\Delta E_{eq} - \Delta E_{meta}| \approx 2k_BT$); however, the magnitude of the energy barrier from the equilibrium orientation to the metastable one ($\Delta E_b - \Delta E_{eq}$) and that from the metastable to equilibrium states ($\Delta E_b - \Delta E_{meta}$) are approximately 45 k_BT (Figure 3c), which is large enough that a spontaneous transition between the two orientations driven by the thermal fluctuation (k_BT) is unlikely to occur. In contrast, for $\beta = 10°$, the magnitude of the energy barrier from the metastable to equilibrium orientations (*i.e.*, from the upright to the tilted orientation) and from the equilibrium to metastable states (*i.e.*, from the tilted to the upright orientation) is $\Delta E_b - \Delta E_{meta} \approx 3k_BT$ and $\Delta E_b - \Delta E_{eq} \approx 400k_BT$, respectively (Figure 3c); therefore, there is a high probability for a spontaneous transition from the upright to the tilted orientation to take place, whereas the reverse transition (*i.e.*, from the tilted to the upright orientation) would be highly unlikely.

The likelihood of Janus ellipsoids undergoing a spontaneous transition between the metastable and equilibrium orientations depends strongly on the particle size. The attachment energy increases with the particle size at a constant AR_e and is given by $\Delta E(c) = \Delta E(c_0) \times (c/c_0)^2$ for Janus ellipsoids where c_0 is the long-axis radius of an ellipsoid of which surface area is $S_0 = 4\pi(10\text{ nm})^2$ (Figure 1). As shown in Figure 3d, the magnitude of the energy barrier from upright to tilted orientations and that from tilted to upright orientations is less than $5k_BT$ (green dotted line in Figure 3d) when the size of the Janus ellipsoids ($32° \leq \beta \leq 40°$, $AR_e = 5$) is $c < 3$ nm. This estimation suggests that these small particles reversibly and spontaneously switch their orientations between the upright and tilted states driven by the thermal fluctuation, k_BT. It is important to note that while Janus ellipsoids with $c = 3$ nm are irreversibly attached to the oil–water interface (*e.g.*, $\Delta E_{eq} \approx 70k_BT$–$85k_BT$), Janus ellipsoids with $c = 1$ nm or smaller could be spontaneously detached from the interface due to relatively small attachment energy ($\Delta E_{eq} < 10k_BT$).[51–53] As the size of the Janus ellipsoids increases, the spontaneous and reversible transition between the two orientations becomes less likely. In the case of a Janus ellipsoid with $c = 5$ nm, $AR_e = 5$, and $\beta = 10°$, for example, $\Delta E_b - \Delta E_{meta}$ is smaller than $1k_BT$, suggesting the high probability of switching its orientation from the upright orientation (metastable state) to the tilted one (equilibrium state). The probability for the reverse transition (*i.e.*, from tilted to upright orientation), however, is less likely due to the higher energy barrier ($\Delta E_b - \Delta E_{eq} \approx 100k_BT$). For larger particles (*e.g.*, $c > 20$ nm), thermally activated spontaneous transitions between the two orientations are unlikely. Thus, some of these larger Janus ellipsoids will adopt the metastable orientation at the oil–water interface.

The distribution of Janus ellipsoids' ($AR_e = 5$ and $\beta = 40°$) orientation at the interface can be quantitatively determined using the Metropolis Monte Carlo simulations (see Methods section) as a function of particle size. As shown in Figure 4a, for larger particles ($c > 10$ nm), the probability of each orientation

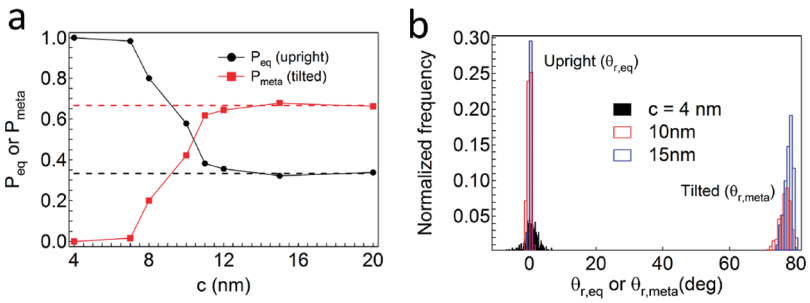

Figure 4. (a) Probability of orientation of Janus ellipsoids ($AR_e = 5$, $\beta = 40°$) as a function of their size. (b) Histogram of upright and tilted orientations for Janus ellipsoids with c = 4, 10, and 15 nm.

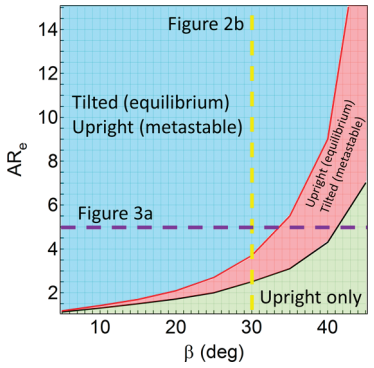

Figure 5. Phase diagram illustrating the effect of AR_e and β on the orientation of Janus ellipsoids at the oil−water interface. The yellow and violet dashed lines correspond to the plots in Figure 2b and Figure 3a, respectively.

(*i.e.*, P_{eq} (upright) and P_{meta} (tilted)) is related to the value of $\theta_{r,b}$ (*i.e.*, orientation angle corresponding to ΔE_b, see Figure 3b), and is given by P (upright) = $\theta_{r,b}/\pi$ and P (tilted) = $(\pi - \theta_{r,b})/\pi$ (dashed lines in Figure 4a). In contrast, in the case of small Janus ellipsoids (c < 10 nm) the energy barrier is comparable to the thermal energy, k_BT. Thus, small Janus ellipsoids in a tilted orientation (*i.e.*, metastable state) can overcome the energy barrier (ΔE_b) and adopt the upright equilibrium orientation. The histogram in Figure 4b also shows that the fraction of Janus ellipsoids trapped in the metastable orientation decreases with the size of Janus ellipsoids.

The effect of AR_e and β on the orientation of Janus ellipsoids at the oil−water interface can be summarized on a phase diagram shown in Figure 5. In general, Janus ellipsoids adopt the upright equilibrium orientation without metastable states at a high β and a low AR_e (light green). Outside this region of single orientation, a coexisting region of two orientations is observed, which can be further divided into two areas. In the area shown in pink, the equilibrium and metastable orientations of interface-trapped Janus ellipsoids correspond to the upright and tilted states, respectively. In the other area shown in light blue, Janus ellipsoids adopt tilted and upright orientations as the equilibrium and metastable states, respectively. Notably, only a tilted orientation would be observed in an extreme case in which a Janus ellipsoid with a high aspect ratio and a very small wettability difference (*e.g.*, $\beta = 0.1°$ and $AR_e = 10$) is trapped at the fluid−fluid interface (not shown in Figure 5). The coexisting regions (light blue and pink areas) become single orientation-dominated regions as the particles become smaller because small particles in metastable states are able to adopt their equilibrium orientation by overcoming the energy barrier between the equilibrium and metastable states (Figure 4).

Janus Dumbbells. Dumbbell particles present a unique opportunity to independently vary the geometry and amphiphilicity of Janus particles, analogous to the packing geometry and the hydrophilic−lipophilic balance (HLB) of molecular surfactants, respectively.[23,24,38] Recent studies have demonstrated the possibility of tuning these characteristics.[23,24] Thus, we investigate the effect of particle geometry and surface properties on the equilibrium orientation of Janus dumbbells.

As shown in Figure 6a, the aspect ratio (AR_d) of Janus dumbbells ($\beta = 30°$) significantly affects their equilibrium orientations (notably, for $AR_d = 1$, the energy profile is identical to the case of a Janus sphere or Janus ellipsoid with $AR_e = 1$ in Figure 2a). As AR_d increases, the Janus boundary rotates out of the oil−water interface plane at equilibrium (Figure 6b and c). It is interesting that the global energy minimum of Janus dumbbells, when $1.6 \leq AR_d \leq 2$, occurs at $33° \leq \theta_{r,eq} \leq 58°$ (Figure 6c); that is, Janus dumbbells adopt tilted orientations. As AR_d is increased, the particle minimizes the attachment energy (eq 7) by increasing S_l, similar to Janus ellipsoids (Figure 2b).

The equilibrium state of Janus dumbbells with $AR_d = 1.5$ changes from a tilted orientation to the upright one for high values of β. The equilibrium angle ($\theta_{r,eq}$) of the particle decreases as β is increased, and the particle eventually prefers the upright orientation when β is approximately 40° or larger, as shown in Figure 6f (note that the equilibrium orientations, $\theta_{r,eq}$, as a function of β are found by minimizing the attachment energy in Figure 6d and e). This implies that in the case of Janus dumbbells with a large β, the configuration is dominated by maximizing the contact area between each region of the particle and its preferred

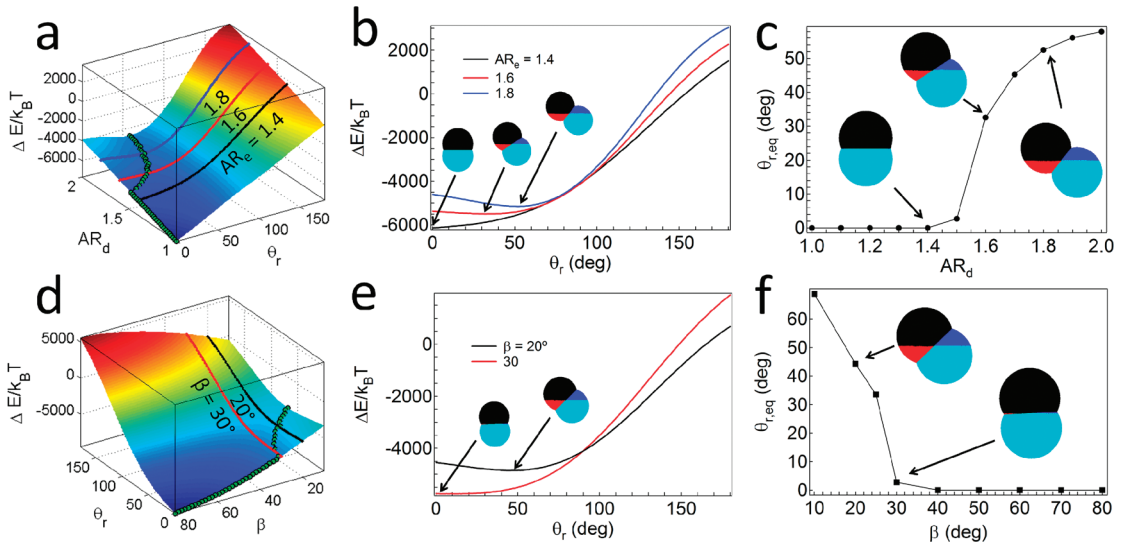

Figure 6. Equilibrium orientations of Janus dumbbells at the oil−water interface. (a) Attachment energy (ΔE) as a function of θ_r and AR_d for $\beta = 30°$. (b) Slices of representative attachment energy profiles from panel a for $AR_e = 1.4$ (black), 1.6 (red), and 1.8 (blue). (c) Equilibrium orientations ($\theta_{r,eq}$) as a function of AR_d. (d) Attachment energy of 3D contour plot as a function of θ_r and β for $AR_d = 1.5$. (e) Slices of representative attachment energy profiles from panel d for $\beta = 20°$ (black) and 30° (red). (f) Equilibrium orientations as a function of β. Green symbols on the 3D plots in panels a and d indicate the global energy minima (ΔE_{eq}) as a function of AR_d and β, respectively.

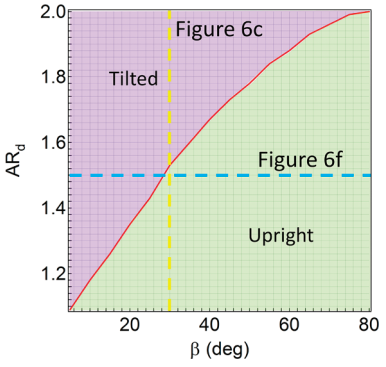

Figure 7. Phase diagram illustrating the effect of AR_d and β on the orientation of Janus dumbbells at the oil−water interface. The yellow and blue dashed lines correspond to the plots in Figure 6c and f, respectively.

fluid phase (*i.e.*, polar in water, S_{PW} and apolar in oil, S_{AO} in Figure 1c and also see eq 7).

The effect of AR_d and β on the equilibrium orientation of Janus dumbbells can be summarized as shown in Figure 7. Janus dumbbells prefer the upright orientation at a small AR_d and a large β, whereas they adopt a tilted orientation under the opposite conditions. Interestingly, unlike Janus ellipsoids, the attachment energy profiles of Janus dumbbells do not possess secondary energy minima. We hypothesize that the absence of a coexisting region in the phase diagram of Janus dumbbells is due to the unique geometry of these particles (*i.e.*, thin "waist" at the Janus boundary). To validate this hypothesis, we compare the attachment energies of Janus dumbbells and spherocylinders with the same aspect ratio and surface area (see Figure S4 for detailed discussion in Supporting Information). Indeed, we find that Janus spherocylinders, under appropriate conditions, have a secondary energy minimum, similar to the case of Janus ellipsoids (Figure S4 in Supporting Information). This result supports our hypothesis that the thin waist of the Janus dumbbells suppresses the existence of metastable orientations.

CONCLUSIONS AND OUTLOOK

We have studied the equilibrium orientation of geometrically and chemically anisotropic particles at an oil−water interface. Our approach enables the prediction of the orientation of nonspherical Janus particles (*i.e.*, ellipsoids and dumbbells) as a function of particle size, aspect ratio, and surface properties. We verified that the flat interface assumption facilitates the determination of the equilibrium orientation of these nonspherical Janus particles at the fluid surface. In general, a larger difference in the wettability of the two regions of Janus particles and a smaller aspect ratio favor the upright orientation. Notably, the existence of the primary and secondary energy minima for Janus ellipsoids indicates that these particles could become kinetically trapped in a metastable state. In this case, our calculation demonstrates that it is critical to control the particle size, at the nanoscale, to enable these particles to overcome energy barrier between the two minima and to adopt their equilibrium orientation. In contrast, only primary energy minimum exists for Janus dumbbells, suggesting that, experimentally, the orientation of Janus dumbbells should be more homogeneous than that of Janus ellipsoids.

The orientation of nonspherical Janus particles likely will have important influence on their ability to stabilize emulsions and modify the rheological properties of fluid interfaces. Thus, the results presented in this study provide important guidance to designing Janus particles with geometry and surface properties suitable for specific applications. The effect of interfacial curvature and packing geometry (*e.g.*, asymmetric Janus dumbbells) on the interfacial behavior of *multiple* Janus particles and, in turn, on the stability of nonspherical Janus particle-covered fluid interfaces warrants further study.[41,43,50] Our current efforts focus on generating particles with controlled anisotropy and surface properties to experimentally investigate their interfacial orientation.[17,22,23,25,27,29,31,32]

METHODS

Attachment Energy Calculation. The attachment energy of a Janus particle from a single fluid phase to a flat oil−water interface is given by

$$\Delta E_{IW} = E_I - E_W \quad \text{from the water phase} \tag{1}$$

$$\Delta E_{IO} = E_I - E_O \quad \text{from the oil phase} \tag{2}$$

where the subscripts I, W, and O denote the interface, water, and oil, respectively.[3,18,19,54] E_W and E_O represent the surface free energy of the system when the particle is completely submerged in water and in oil, respectively. E_I represents the surface free energy of the system when the particle is attached to the interface. Each surface free energy term can be expressed as

$$\begin{aligned} E_W &= S_A\gamma_{AW} + S_P\gamma_{PW} + S_{OW}^{(1)}\gamma_{OW} \\ E_O &= S_A\gamma_{AO} + S_P\gamma_{PO} + S_{OW}^{(1)}\gamma_{OW} \\ E_I &= S_{AO}\gamma_{AO} + S_{AW}\gamma_{AW} + S_{PO}\gamma_{PO} + S_{PW}\gamma_{PW} + S_{OW}^{(2)}\gamma_{OW} \end{aligned} \tag{3}$$

where γ_{ij} is the interfacial tension between i and j, and the subscripts, A and P indicate apolar and polar surfaces of the Janus particle, respectively.[3,18,19] $S_{OW}^{(1)}$ and $S_{OW}^{(2)}$ represent the surface area of the oil−water interface in the absence and in the presence of the Janus particle, respectively. When the particle attaches to the oil−water interface, the surface area exposed to each fluid phase becomes $S_A = S_{AW} + S_{AO}$ and $S_P = S_{PW} + S_{PO}$. Combining eq 1 and 2 with eq 3 yields,

$$\Delta E_{IW} = S_{AO}(\gamma_{AO} - \gamma_{AW}) + S_{PO}(\gamma_{PO} - \gamma_{PW}) - S_I\gamma_{OW} \tag{4}$$

$$\Delta E_{IO} = S_{AW}(\gamma_{AW} - \gamma_{AO}) + S_{PW}(\gamma_{PW} - \gamma_{PO}) - S_I\gamma_{OW} \tag{5}$$

where S_I is the area of the oil−water interface occupied by the particle when it is attached to the interface (*i.e.*, $S_I = S_{OW}^{(1)} - S_{OW}^{(2)}$). Young's equations for homogeneous polar and apolar spherical particles are given by

$$\begin{aligned} \gamma_{OW}\cos\theta_P &= \gamma_{PO} - \gamma_{PW} \\ \gamma_{OW}\cos\theta_A &= \gamma_{AO} - \gamma_{AW} \end{aligned} \tag{6}$$

where θ_P and θ_A are the three-phase contact angles of polar and apolar particles, respectively (see Figure 1b). On the basis of eqs 4−6, the attachment energy from the water and oil phase can be expressed as

$$\Delta E_{IW} = \gamma_{OW}(S_{AO}\cos\theta_A + S_{PO}\cos\theta_P - S_I) \tag{7}$$

$$\Delta E_{IO} = -\gamma_{OW}(S_{AW}\cos\theta_A + S_{PW}\cos\theta_P + S_I) \tag{8}$$

The equilibrium orientation of the Janus particle is determined by minimizing ΔE_{IW} or ΔE_{IO} as a function of orientation angle (θ_r). A detailed procedure is described below. Note that eq 7 and 8 will result in the same equilibrium orientation (*i.e.*, $\cos\theta_A = -\cos\theta_P$). Unless otherwise noted, we use eq 7 to determine the equilibrium orientation of nonspherical Janus particles.

Surface Area Calculation. We numerically calculate the surface area of an interface-trapped nonspherical Janus particle exposed to each fluid phase. A large number of random points (N_{tot}) are homogeneously generated on the particle surface. The fraction of the points ($P_{ij} = N_{ij}/N_{tot}$) that are found in one of four possible conditions—apolar surface in oil ($i = A$ and $j = O$), apolar surface in water ($i = A$ and $j = W$), polar surface in oil ($i = P$ and $j = O$), and polar surface in water ($i = P$ and $j = W$)—enables the calculation of the surface area using $S_{ij} = P_{ij}\cdot S_{tot}$ (S_{tot} = total surface area). In this process, we assume that the contact line between the particle and the interface is smooth.[3,18,19] The effect of line tension at the contact line is negligible since we consider particles that are larger than 1 nm.[18,19] We also neglect the effect of gravity-induced interface deformation, which may be important for particles that are larger than hundreds of micrometers.[55] To facilitate the estimation of equilibrium orientation of nonspherical Janus particles at the oil−water interface, we perform the calculation of attachment energy assuming that the oil−water interface around a Janus particle remains flat (the validation of this assumption is described in Supporting Information).

Equilibrium Orientation. To find the equilibrium orientation of a Janus particle at an oil−water interface, we calculate the attachment energy (ΔE) using eq 7. Note that the use of either eq 7 or eq 8 results in the same equilibrium orientation, as discussed above. For a nonspherical Janus particle at a flat interface with a given set of parameters (*i.e.*, a constant β and AR_e for Janus ellipsoids, and a constant β and AR_d for Janus dumbbells), we calculate the attachment energy as a function of θ_r with the increment of less than 1°; the equilibrium orientation angle ($\theta_{r,eq}$) can be found by finding the minimum attachment energy (ΔE_{eq}).

Orientation Angle Distribution of Janus Ellipsoids. Metropolis Monte Carlo (MC) simulation is used to estimate the probability distribution of orientation angle of Janus ellipsoids (Figure 4). We assume that the particles initially have a random orientation (0−2π). Particles are allowed to undergo random rotation ($d\theta_{r,MC} \leq \pm 4°$), and the probability of each random angular displacement is determined using the energy profile we calculated. We assume that the vertical displacement is negligible (*i.e.*, $\cos\theta_A = -\cos\theta_P$), as discussed earlier. To obtain the statistical confidence, the number of particles simulated is larger than 500. We use at least 500 MC cycles to determine the orientation of a Janus particle at the oil−water interface.

Acknowledgment. Acknowledgment is made to the Donors of the American Chemical Society Petroleum Research Fund for support of this research. This work was also partly supported by an NSF CAREER Award (DMR-1055594), the PENN MRSEC DMR11-20901 through the National Science Foundation and the University Research Foundation (URF) of the University of Pennsylvania.

Supporting Information Available: Validation of the flat interface assumption (FIA) for Janus ellipsoids and dumbbells. Calculation of the attachment energy of spherocylinders. This material is available free of charge *via* the Internet at http://pubs.acs.org.

REFERENCES AND NOTES

1. Casagrande, C.; Veyssié, M. Grains Janus": Réalisation et Premières Observations Des Propriétiés Interfaciales. *C. R. Acad. Sci., Paris* **1988**, *306*, 1423–1425.

2. Casagrande, C.; Fabre, P.; Raphael, E.; Veyssié, M. "Janus Beads": Realization and Behaviour at Water/Oil Interfaces. *Europhys. Lett.* **1989**, *9*, 251–255.
3. Ondarçuhu, T.; Fabre, P.; Raphaël, E.; Veyssié, M. Specific Properties of Amphiphilic Particles at Fluid Interfaces. *J. Phys. (Paris)* **1990**, *51*, 1527–1536.
4. de Gennes, P. G. Soft Matter. *Rev. Mod. Phys.* **1992**, *64*, 645–648.
5. Chen, Q.; Whitmer, J. K.; Jiang, S.; Bae, S. C.; Luijten, E.; Granick, S. Supracolloidal Reaction Kinetics of Janus Spheres. *Science* **2011**, *331*, 199–202.
6. Forster, J. D.; Park, J.-G.; Mittal, M.; Noh, H.; Schreck, C. F.; O'Hern, C. S.; Cao, H.; Furst, E. M.; Dufresne, E. R. Assembly of Optical Scale Dumbbells into Dense Photonic Crystals. *ACS Nano* **2011**, *5*, 6695–6700.
7. Gangwal, S.; Cayre, O. J.; Velev, O. D. Dielectrophoretic Assembly of Metallodielectric Janus Particles in AC Electric Fields. *Langmuir* **2008**, *24*, 13312–13320.
8. Gangwal, S.; Pawar, A.; Kretzschmar, I.; Velev, O. D. Programmed Assembly of Metallodielectric Patchy Particles in External AC Electric Fields. *Soft Matter* **2010**, *6*, 1413–1418.
9. Ku, J.; Aruguete, D. M.; Alivisatos, A. P.; Geissler, P. L. Self-Assembly of Magnetic Nanoparticles in Evaporating Solution. *J. Am. Chem. Soc.* **2010**, *133*, 838–848.
10. McConnell, M. D.; Kraeutler, M. J.; Yang, S.; Composto, R. J. Patchy and Multiregion Janus Particles with Tunable Optical Properties. *Nano Lett.* **2010**, *10*, 603–609.
11. Jiang, S.; Chen, Q.; Tripathy, M.; Luijten, E.; Schweizer, K. S.; Granick, S. Janus Particle Synthesis and Assembly. *Adv. Mater.* **2010**, *22*, 1060–1071.
12. Zhang, L.; Zhu, Y. Dielectrophoresis of Janus Particles under High Frequency AC-Electric Fields. *Appl. Phys. Lett.* **2010**, *96*, 141902–3.
13. Glotzer, S. C.; Solomon, M. J. Anisotropy of Building Blocks and Their Assembly into Complex Structures. *Nat. Mater.* **2007**, *6*, 557–562.
14. Grzelczak, M.; Vermant, J.; Furst, E. M.; Liz-Marzán, L. M. Directed Self-Assembly of Nanoparticles. *ACS Nano* **2010**, *4*, 3591–3605.
15. Howse, J. R.; Jones, R. A. L.; Ryan, A. J.; Gough, T.; Vafabakhsh, R.; Golestanian, R. Self-Motile Colloidal Particles: From Directed Propulsion to Random Walk. *Phys. Rev. Lett.* **2007**, *99*, 048102–4.
16. Jiang, H.-R.; Yoshinaga, N.; Sano, M. Active Motion of a Janus Particle by Self-Thermophoresis in a Defocused Laser Beam. *Phys. Rev. Lett.* **2010**, *105*, 268302–4.
17. Hong, Y.; Blackman, N. M. K.; Kopp, N. D.; Sen, A.; Velegol, D. Chemotaxis of Nonbiological Colloidal Rods. *Phys. Rev. Lett.* **2007**, *99*, 178103–4.
18. Binks, B. P.; Fletcher, P. D. I. Particles Adsorbed at the Oil-Water Interface: A Theoretical Comparison between Spheres of Uniform Wettability and "Janus" Particles. *Langmuir* **2001**, *17*, 4708–4710.
19. Jiang, S.; Granick, S. Janus Balance of Amphiphilic Colloidal Particles. *J. Chem. Phys.* **2007**, *127*, 161102–4.
20. Faria, J.; Ruiz, M. P.; Resasco, D. E. Phase-Selective Catalysis in Emulsions Stabilized by Janus Silica-Nanoparticles. *Adv. Synth. Catal.* **2011**, *352*, 2359–2364.
21. Fujimoto, K.; Nakahama, K.; Shidara, M.; Kawaguchi, H. Preparation of Unsymmetrical Microspheres at the Interfaces. *Langmuir* **1999**, *15*, 4630–4635.
22. Güell, O.; Sagués, F.; Tierno, P. Magnetically Driven Janus Micro-Ellipsoids Realized *via* Asymmetric Gathering of the Magnetic Charge. *Adv. Mater.* **2011**, *23*, 3674–3679.
23. Kim, J.-W.; Larsen, R. J.; Weitz, D. A. Synthesis of Nonspherical Colloidal Particles with Anisotropic Properties. *J. Am. Chem. Soc.* **2006**, *128*, 14374–14377.
24. Kim, J.-W.; Lee, D.; Shum, H. C.; Weitz, D. A. Colloid Surfactants for Emulsion Stabilization. *Adv. Mater.* **2008**, *20*, 3239–3243.
25. Roh, K.-H.; Martin, D. C.; Lahann, J. Biphasic Janus Particles with Nanoscale Anisotropy. *Nat. Mater.* **2005**, *4*, 759–763.
26. Wang, B.; Li, B.; Ferrier, R. C. M.; Li, C. Y. Polymer Single Crystal Templated Janus Nanoparticles. *Macromol. Rapid Commun.* **2010**, *31*, 169–175.
27. Zhang, L.; Zhang, F.; Wang, Y.-S.; Sun, Y.-L.; Dong, W.-F.; Song, J.-F.; Huo, Q.-S.; Sun, H.-B. Magnetic Colloidosomes Fabricated by Fe_3O_4–SiO_2 Hetero-nanorods. *Soft Matter* **2011**, *7*, 7375–7381.
28. Zhang, Z.; Pfleiderer, P.; Schofield, A. B.; Clasen, C.; Vermant, J. Synthesis and Directed Self-Assembly of Patterned Anisometric Polymeric Particles. *J. Am. Chem. Soc.* **2010**, *133*, 392–395.
29. Choi, C.-H.; Lee, J.; Yoon, K.; Tripathi, A.; Stone, H. A.; Weitz, D. A.; Lee, C.-S. Surface-Tension-Induced Synthesis of Complex Particles Using Confined Polymeric Fluids. *Angew. Chem., Int. Ed.* **2010**, *49*, 7748–7752.
30. Lee, D.; Weitz, D. A. Nonspherical Colloidosomes with Multiple Compartments from Double Emulsions. *Small* **2009**, *5*, 1932–1935.
31. Ruhland, T. M.; Gröschel, A. H.; Walther, A.; Müller, A. H. E. Janus Cylinders at Liquid–Liquid Interfaces. *Langmuir* **2011**, *27*, 9807–9814.
32. Buck, M. R.; Bondi, J. F.; Schaak, R. E. A Total-Synthesis Framework for the Construction of High-Order Colloidal Hybrid Nanoparticles. *Nat. Chem.* **2012**, *4*, 37–44.
33. Ho, C. C.; Keller, A.; Odell, J. A.; Ottewill, R. H. Preparation of Monodisperse Ellipsoidal Polystyrene Particles. *Colloid Polym. Sci.* **1993**, *271*, 469–479.
34. Keville, K. M.; Franses, E. I.; Caruthers, J. M. Preparation and Characterization of Monodisperse Polymer Microspheroids. *J. Colloid Interface Sci.* **1991**, *144*, 103–126.
35. Loudet, J. C.; Alsayed, A. M.; Zhang, J.; Yodh, A. G. Capillary Interactions between Anisotropic Colloidal Particles. *Phys. Rev. Lett.* **2005**, *94*, 018301–4.
36. Madivala, B.; Fransaer, J.; Vermant, J. Self-Assembly and Rheology of Ellipsoidal Particles at Interfaces. *Langmuir* **2009**, *25*, 2718–2728.
37. Mock, E. B.; De Bruyn, H.; Hawkett, B. S.; Gilbert, R. G.; Zukoski, C. F. Synthesis of Anisotropic Nanoparticles by Seeded Emulsion Polymerization. *Langmuir* **2006**, *22*, 4037–4043.
38. Israelachvili, J. N. *Intermolecular and Surface Forces*, 3rd ed.; Academic Press: New York, 2011.
39. Cheung, D. L.; Bon, S. A. F. Stability of Janus Nanoparticles at Fluid Interfaces. *Soft Matter* **2009**, *5*, 3969–3976.
40. Fan, H.; Resasco, D. E.; Striolo, A. Amphiphilic Silica Nanoparticles at the Decane–Water Interface: Insights from Atomistic Simulations. *Langmuir* **2011**, *27*, 5264–5274.
41. Hirose, Y.; Komura, S.; Nonomura, Y. Adsorption of Janus Particles to Curved Interfaces. *J. Chem. Phys.* **2007**, *127*, 054707–5.
42. Glaser, N.; Adams, D. J.; Boker, A.; Krausch, G. Janus Particles at Liquid–Liquid Interfaces. *Langmuir* **2006**, *22*, 5227–5229.
43. Park, B. J.; Brugarolas, T.; Lee, D. Janus Particles at an Oil–Water Interface. *Soft Matter* **2011**, *7*, 6413–6417.
44. Park, B. J.; Furst, E. M. Attractive Interactions Between Colloids at the Oil–Water Interface. *Soft Matter* **2011**, *7*, 7676–7682.
45. Park, B. J.; Pantina, J. P.; Furst, E. M.; Oettel, M.; Reynaert, S.; Vermant, J. Direct Measurements of the Effects of Salt and Surfactant on Interaction Forces between Colloidal Particles at Water–Oil Interfaces. *Langmuir* **2008**, *24*, 1686–1694.
46. Park, B. J.; Vermant, J.; Furst, E. M. Heterogeneity of the Electrostatic Repulsion Between Colloids at the Oil–Water Interface. *Soft Matter* **2010**, *6*, 5327–5333.
47. Reynaert, S.; Moldenaers, P.; Vermant, J. Control over Colloidal Aggregation in Monolayers of Latex Particles at the Oil–Water Interface. *Langmuir* **2006**, *22*, 4936–4945.
48. Although we calculate attachment energy of Janus particles whose surface area is equivalent to that of a 10 nm spherical particle, the attachment energy of a particle with different surface area can be readily calculated (see "Attachment Energy Calculation" in the Methods section).
49. 2D energy profiles (ΔE) as a function of θ_r for several different values of AR_e are calculated and are subsequently interpolated to generate 3D contour plots.

50. Brugarolas, T.; Park, B. J.; Lee, D. Generation of Amphiphilic Janus Bubbles and Their Behavior at an Air–Water Interface. *Adv. Funct. Mater.* **2011**, *21*, 3924–3931.
51. Du, K.; Glogowski, E.; Emrick, T.; Russell, T. P.; Dinsmore, A. D. Adsorption Energy of Nano- and Microparticles at the Liquid–Liquid Interfaces. *Langmuir* **2010**, *26*, 12518–12522.
52. Lin, Y.; Skaff, H.; Emrick, T.; Dinsmore, A. D.; Russell, T. P. Nanoparticle Assembly and Transport at Liquid–Liquid Interfaces. *Science* **2003**, *299*, 226–229.
53. The contribution of line tension is not considered here; however, it may become significant for particles that are smaller than 1 nm (see refs 18 and 19).
54. Binks, B. P.; Horozov, T. S. *Colloidal Particles at Liquid Interfaces*; Cambridge University Press: New York, 2006.
55. Vassileva, N. D.; vandenEnde, D.; Mugele, F.; Mellema, J. Capillary Forces between Spherical Particles Floating at a Liquid–Liquid Interface. *Langmuir* **2005**, *21*, 11190–11200.